(U-Th)/He dating of supergene iron (oxyhydr-)oxides of the Nefza-Sejnane district (Tunisia)

YANS, Johan; Verhaert, Michele; Gautheron, Cécile; Antoine, Pierre-Olivier; Moussi, Béchir; Dekoninck, Augustin; Decrée, Sophie; Chaftar, R.; HATIRA, N.; Dupuis, Christian; Pinna-Jamme, Rosella; Jamoussi, Fakher

Published in:
Minerals

DOI:
10.3390/min11030260

Publication date:
2021

Document Version
Publisher's PDF, also known as Version of record

minerals

MDPI

Article

(U-Th)/He Dating of Supergene Iron (Oxyhydr-)Oxides of the Nefza-Sejnane District (Tunisia): New Insights into Mineralization and Mammalian Biostratigraphy

Johan Yans [1,*], Michèle Verhaert [1], Cecile Gautheron [2], Pierre-Olivier Antoine [3], Béchir Moussi [4], Augustin Dekoninck [1], Sophie Decrée [5], Hédi-Ridha Chaftar [6], Nouri Hatira [7], Christian Dupuis [8], Rosella Pinna-Jamme [2] and Fakher Jamoussi [4]

1 Department of Geology, Institute of Life, Earth and Environment ILEE, University of Namur, 5000 Namur, Belgium; michele-alexandra.verhaert@unamur.be (M.V.); augustin.dekoninck@unamur.be (A.D.)
2 Université Paris-Saclay, CNRS, GEOPS, 91405 Orsay, France; cecile.gautheron@universite-paris-saclay.fr (C.G.); rosella.pinna@universite-paris-saclay.fr (R.P.-J.)
3 Institut des Sciences de l'Evolution de Montpellier, CNRS, IRD, EPHE, Université de Montpellier, Place Eugène Bataillon, CEDEX 05, 34095 Montpellier, France; pierre-olivier.antoine@umontpellier.fr
4 Water Researches and Technologies Center CERTE, Technopôle de Borj Cedria BP 273, Soliman 8020, Tunisia; bechirmoussi2007@gmail.com (B.M.); fakher.jamoussi@certe.rnrt.tn (F.J.)
5 Royal Belgian Institute of Natural Sciences, Geological Survey of Belgium, 1000 Brussels, Belgium; sdecree@naturalsciences.be
6 Office National des Mines, Tunis 2035, Tunisia; ridhachaftar@yahoo.fr
7 Faculté des Sciences de Bizerte, Zarzouna 7021, Tunisia; nhatira@gmail.com
8 UMons, Département de Géologie Fondamentale et Appliquée, rue de Houdain, 7000 Mons, Belgium; Christian.DUPUIS@umons.ac.be
* Correspondence: johan.yans@unamur.be

Abstract: The mining district of Nefza-Sejnane (Tunisia) encloses numerous ores and raw material deposits, all formed in relation with successive Fe-rich fluids of meteoric and/or hydrothermal origins. Here, for the first time in Tunisia, (U-Th)/He ages were obtained on supergene goethite from various localities/deposits of the district highlight direct dating of significant weathering episodes during late Tortonian and late Pleistocene. These weathering events are most likely associated with favorable conditions that combine (i) wet climate displaying sufficient meteoric water/fluid; and (ii) regional exhumation, due to large-scale vertical lithospheric movements enhancing the percolation of fluids. Matched with previous works, these results refine the stratigraphic frame for the polymetallic mineralization and clay deposits in the district, confirming the influence of meteoric fluids circulation during the late Cenozoic. As a consequence of the new (U-Th)/He data, we moreover propose a taxonomic and stratigraphic revision of the well-known mammalian fauna from the Fe-rich Douahria locality, suggesting an early Tortonian age for the fossils, i.e., prior to the first episode of meteoric event in the area.

Keywords: (U-Th)/He; goethite; supergene; Douahria mammalian fauna; Tunisia

Citation: Yans, J.; Verhaert, M.; Gautheron, C.; Antoine, P.-O.; Moussi, B.; Dekoninck, A.; Decrée, S.; Chaftar, H.-R.; Hatira, N.; Dupuis, C.; et al. (U-Th)/He Dating of Supergene Iron (Oxyhydr-)Oxides of the Nefza-Sejnane District (Tunisia): New Insights into Mineralization and Mammalian Biostratigraphy. *Minerals* **2021**, *11*, 260. https://doi.org/10.3390/min11030260

Academic Editor: Harald G. Dill

Received: 21 January 2021
Accepted: 24 February 2021
Published: 3 March 2021

1. Introduction

The mining district of Nefza-Sejnane contains numerous ores and raw material deposits, including the Zn–Pb mineralization of Sidi Driss, the vertebrate-bearing Douahria basin that hosts a SEDEX deposit [1], the halloysite-bearing iron deposit of Tamra Formation [2–5], the Fe-LREE-U enriched breccia of Oued Belif [5], and kaolinitic clays of the late Oligocene Numidian Flysch Formation [6,7]; (Figures 1 and 2). From the Miocene onwards, these deposits experienced successive circulations of Fe-rich fluids of mixed meteoric and hydrothermal origins. The hydrothermal activity resulted from a relatively high geothermal gradient and Miocene magmatic rocks of the area [8]. Using geochemical

arguments, Decrée et al. (2014) demonstrated that emplacement of magmatic rocks in the Nefza district has enhanced hydrothermal fluid circulations, leading to the deposition of polymetallic mineralization [9]. In addition, significant periods of weathering are confirmed by (i) pedogenesis on sediments within small basins such as in Tamra basin and the deposition of the subaerial Tamra Formation [2]; and (ii) late supergene fluids leading to the formation of botryoidal or euhedral goethite [4,5]. The nature and role of meteoric circulations in metal enrichment of the area has already been stressed by Decrée et al. [1,2] and discussed by Dekoninck et al. [4] using δD and $\delta^{18}O$ on halloysite-kaolinite and Fe (oxyhydr-)oxides, and by Decrée et al. [10] using iron isotopes and chemical composition of Fe-(oxi)hydroxides. However, ages of these meteoric influences in this area are still lacking, jeopardizing the regional integration of the ore formation. Furthermore, the Douahria Fe-deposit contains the famous "Pikermian" vertebrate fauna, including a rhinocerotid, a giraffid, and an anthracotheriid originally described by Roman and Solignac [11] in a ferruginous crust. Here we provide, for the first time in Tunisia, new (U-Th)/He ages on goethite (GHe ages) associated with weathering processes in the vertebrate-bearing Nefza-Sejnane polymetallic mining district. Matched with previous data, these new investigations allow us to discuss (i) the influence of meteoric fluids in the formation of ore deposits in this important mining district of Tunisia, and (ii) the role of geodynamic and climatic parameters in weathering processes at a regional scale. Moreover, we propose a global revision of the mammalian assemblage, aiming at providing updated taxonomic assignments for the concerned remains and discussing their biostratigraphic outputs, in order to further discuss GHe ages and paleontological dating.

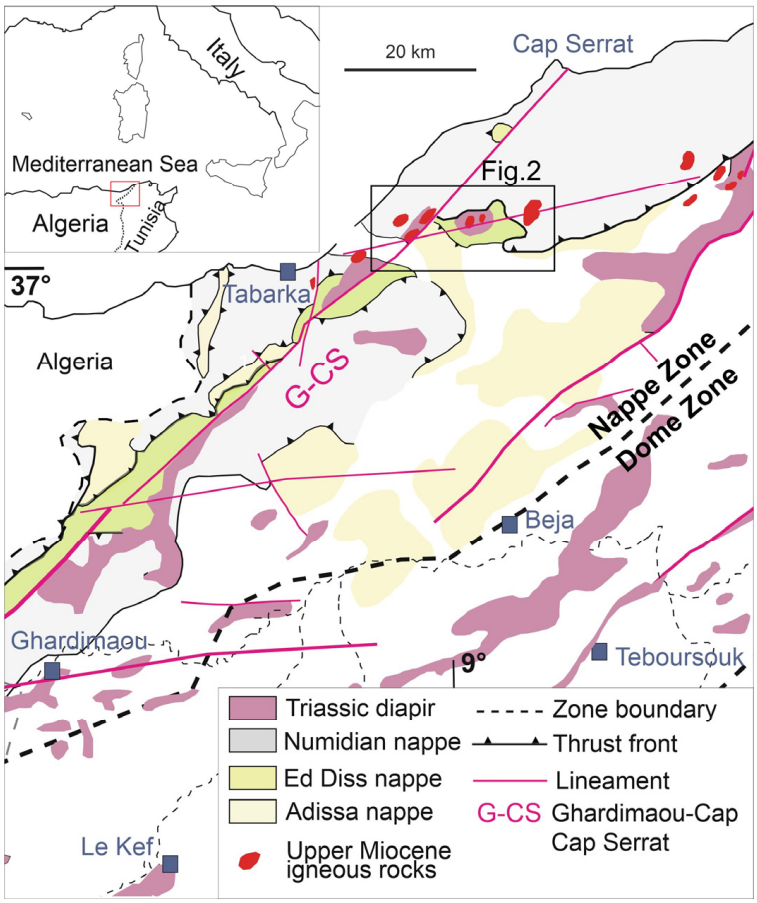

Figure 1. Tectonic map of central and northern Tunisia, showing the location of the studied area (Figure 2; modified after references [4,12–14].

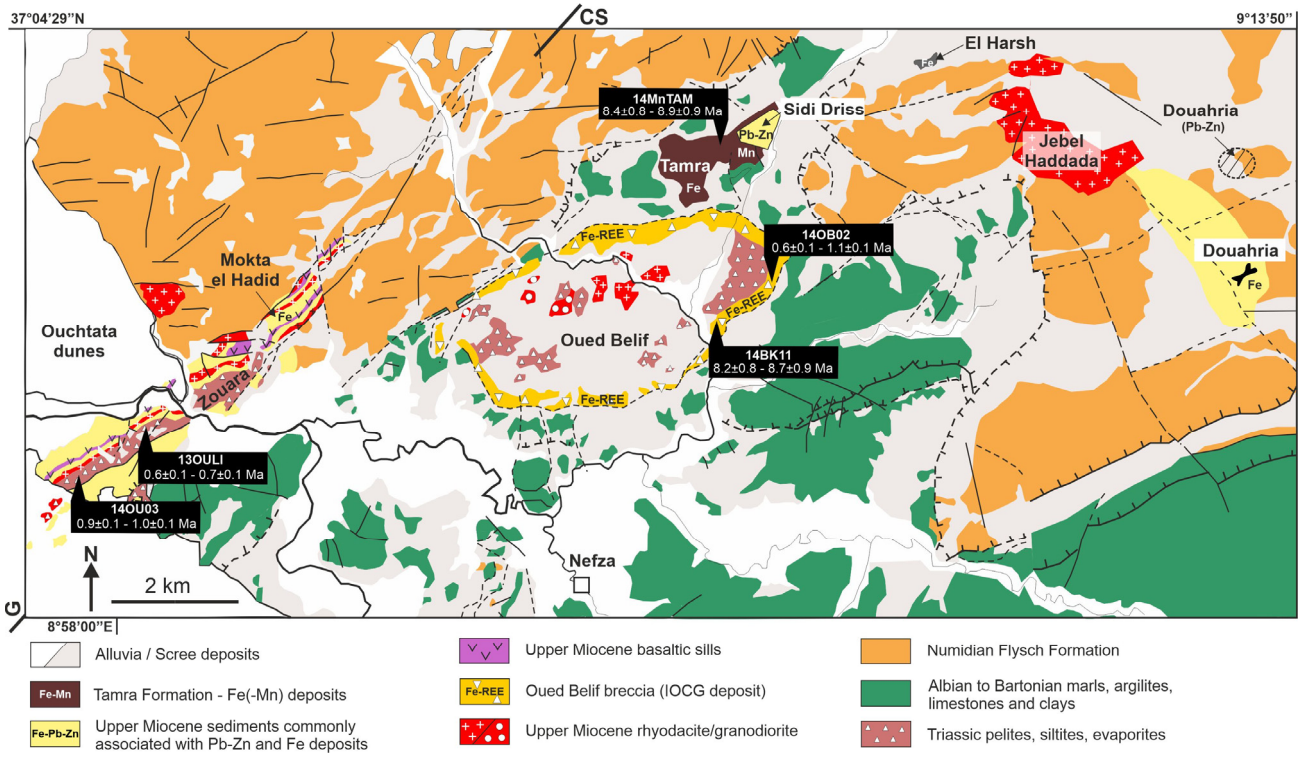

Figure 2. Simplified geologic map of the Nefza-Sejnane district, Tunisia (modified after reference [5], showing the location and (U-Th)/He corrected ages of the supergene goethite. G-CS = Ghardimaou Cap Serrat sinistral fault zone.

2. Geological Setting

The Nefza-Sejnane mining district is located in the Tellian "Nappe Zone" of Northern Tunisia (Figures 1 and 2). The district is characterized by the occurrence of late Cenozoic mineral deposits, overlying a substratum comprising folded marls Albian to late Priabonian in age, and Chattian–Burdigalian Numidian Flysch Formation [15], which are present as thrust sheets in the Tellian "Nappe Zone" [16]. The regional felsic sub-volcanic rocks were emplaced between 12.9 ± 0.5 Ma and 8.2 ± 0.4 Ma (Serravallian to Tortonian; e.g., [8]), while basaltic flows of the Zouara basin (Figure 2) were dated between 8.4 ± 0.4 Ma and 6.4 ± 0.2 Ma [17]. The Ghardimaou-Cap Serrat (G-CS) sinistral fault zone, a major regional structure guiding Alpine tectonics at the tectonic plate scale, and the regional N80°E lineaments controlled the magmatism and subsequent mineralization (Figures 1 and 2; [14]). The first notable mineralization event in the area was associated with a major brecciation episode that led to the formation of the ring-shaped Oued Belif LREE-U hematite breccia [5]. The origin of this breccia is most likely related to the mixing of magmatic-hydrothermal fluids and basinal (evaporite) brines. A K-Fe alteration event, slightly predating the main mineralization, is dated at 9.2 ± 0.3 Ma using K-Ar method on K-feldspars [5]. The main Fe-LREE-U mineralization is coeval with a major episode of brecciation, most likely associated with the emplacement of the Oued Belif rhyolite intrusion. The remaining voids are filled with goethite, which, in some areas, is mixed with kaolinite and Ba-Mn oxide. The two SEDEX deposits (Sidi Driss and Douahria; Figure 2) are formed through thermally-driven fluid circulations related to magmatism and reactivation of shear zones during late Miocene extension in small basins (Decrée et al., 2016 [14]). The Pb-Zn ore of Sidi Driss is correlated with the stratified Fe-ore of Douahria, which yielded a large mammalian assemblage, late Miocene in age (originally spelled Douaria; e.g., [18–20]). The Tamra basin, unconformably overlying the Sidi Driss basin, is the host for iron mineralization in the form of a 50 m thick succession (Tamra Formation) of iron hydroxide-stained sediments together with kaolinite-halloysite lenses [1,3,4]. Previous datings on hollandite [$Ba(Mn^{4+},Mn^{2+})_8O_{16}$] and coronadite [$Pb(Mn^{4+},Mn^{2+})_8O_{16}$] from Tamra yielded Pliocene K-Mn ages [2]. The dated

K-Mn oxides relate to mineralizing events closely connected with hydrothermal circulation and leaching of underlying mineralization of the Sidi Driss Pb–Zn SEDEX type deposit [2]. At Tamra, the δD and $\delta^{18}O$ of halloysite-kaolinite are not in equilibrium with the potential Miocene-Pliocene meteoric fluids, confirming that they could be related to fluid-rock interactions with the underlying ores, marls, and/or skarns [4]. Late mineralization of galena, pyrite, and siderite in sub-vertical fractures cut the whole sequence of the district and are associated with a new hydrothermal event, still active in the area with numerous hot springs from 35 °C up to 70 °C and regional thermal gradients up to 100 °C/km [8]. Recent circulation of hydrothermal fluids is moreover confirmed by K-Ar dating of adularia at c. 0 Ma in the Oued Belif breccia [5].

3. Materials and Methods

Samples of iron (oxyhydr-)oxides were collected in the Tamra Fe-mine, the Boukhchiba Fe-mine, the Oued Belif Fe-LREE-U breccia, and the Ouchtata area-Zouara basin (Figure 2; Table 1) during field campaigns in 2013 and 2014. Sample 14MnTAM was collected in the upper part of the Tamra mine, within the manganiferous zone (see field pictures and log in reference [2]. It contains pure, well-crystallized goethite with botryoidal texture (Figure 3A,B) that formed during the pedogenesis affecting the Tamra Formation [4]. The 14TAM07 sample, also collected in the Tamra mine (see reference [2]), shows a mixture of goethite and hematite, with potential influences of both weathering and hydrothermal origins, as attested by the occurrence of hematite and Mn(Pb)-oxides (Figure 3C,D). The 13NEFZA sample, also collected in the Tamra mine, corresponds to Fe-indurations of the intermediate part of the sequence defined by Decrée et al. [2]. This sample contains hematite and displays hydrothermal influences according to δD and $\delta^{18}O$ data from Dekoninck et al. [4] (their samples CP04-3 and CP04-35 are very similar to our sample 13NEFZA). The 14BK11 sample comes from a mineralized vein in the Boukhchiba Fe-mine (Figure 2), clearly cross-cutting the Fe-LREE-U-rich breccia described in Decrée et al. [5] and field pictures herein). The sample contains very pure, well-crystallized, and homogeneous goethite (Figure 3E,F), which precipitated in equilibrium with meteoric waters [4]. The 14OU03 and the 13OULI samples were collected in the Ouchtata area (Figure 2). They consist of several generations of goethite pseudomorphosing grains of pyrite of the Triassic sediments. "Ouchtata" sample in reference [4], similar to 13OULI sample, was associated with meteoric fluids by the latter authors. Sample 14OB02 was collected in a mineralized vein of the Oued Belif locality. It contains goethite, mixed with euhedral quartz and K-feldspars (Figure 3G,H). The goethite of this sample was considered as supergene (formed below the water table) by Decrée et al. [5]. The isotopic data of this sample are consistently away from the meteoric equilibrium water line [4], due to mixing with quartz and K-feldspars. Ferruginous crust from the mammal-bearing Douahria site was also sampled in order to perform (U-Th)/He dating. The latter, however, contains large amounts of mixed hydrothermal Fe-Mn phases, and could thus not be analyzed with the (U-Th)/He method.

Table 1. Sampling site, geological characterization, and (U-Th)/He data of analyzed samples. N.A. = not analyzed.

Geological Characterization				(U-Th)/He Data											
Geological Context	**Mineralogy**	**Geographical Coordinates**	**Interpretation δD-δ^{18}O [4]**	**Label**	**Weight (mg)**	**^{4}He (nccSTP */g)**	**±1σ ** (nccSTP/g)**	**U (ppm)**	**Th (ppm)**	**eU *** (ppm)**	**Th/U**	**Raw Age (Ma)**	**±1σ (Ma)**	**Age (Ma) + 10%**	**±10% (Ma) 1σ**
Fe ore in breccia [5]	Euhedral goethite in vein	N 37°02′1.7″; E 9°06′31.5″	In equilibrium with meteoric waters	14BK-11-A	10.4	1517	30	1.7	0.02	1.7	0.01	7.5	0.4	8.2	0.8
				14BK-11-B	13.3	1892	38	1.9	0.23	2.0	0.12	7.9	0.4	8.7	0.9
Tamra Fe ore [2]	Botryoidal goethite in Mn zone	N37°3′27.76″; E 9°6′14.10″	In equilibrium with meteoric waters	14MN-TAM-A	6.6	1039	21	1.1	0.02	1.1	0.02	8.1	0.4	8.9	0.9
				14MN-TAM-B	17.9	671	13	0.7	0.02	0.7	0.03	7.9	0.4	8.7	0.9
				14MN-TAM-C	9.7	984	20	1.1	0.04	1.1	0.04	7.7	0.4	8.4	0.8
Tamra Fe ore [2]	Goethite-hematite poorly crystallized, rich in Mn, mixing of several phases	N 37°03′25.6″; E 9°06′4.8″	In equilibrium with meteoric waters	14TAM-07-A	11.0	210	4	0.4	0.73	0.6	1.81	3.0	0.2	3.3.	0.3
				14TAM-07-B	12.3	371	7	0.4	0.72	0.6	1.86	5.5	0.3	6.1	0.6
				14TAM-07-C	13.7	381	8	0.4	0.63	0.6	1.57	5.7	0.3	6.3	0.6
Tamra Fe ore [2]	Goethite-hematite in vein	N 37°3′23.77″; E 9°6′4.48″	N.A (similar and close to samples CP04-3 and CP04-35, not in equilibrium with meteoric waters)	13NEFTA-A	11.4	165	3	0.6	0.06	0.6	0.11	2.4	0.1	2.6	0.3
				13NEFTA-B	7.6	56	1	0.5	0.03	0.5	0.07	0.9	0.0	1.0	0.1
				13NEFTA-C	11.5	225	4	0.9	0.06	0.9	0.07	2.0	0.1	2.3	0.2
Weathered Triassic	Goethite-Pseudomorphose of pyrite	N 37°00′38.8″; E 8°58′9.4″	sample "Ouchtata" in ref. [4], in equilibrium with meteoric waters	14OU03-1	0.9	230	5	2.3	0.02	2.3	0.01	0.8	0.0	0.9	0.1
				14OU03-2	0.5	202	4	1.9	0.06	1.9	0.03	0.9	0.0	0.9	0.1
				14OU03-3	0.5	400	8	3.8	0.05	3.8	0.01	0.9	0.0	1.0	0.1
Weathered Triassic	Euhedral goethite	N 37°00′38.8″; E 8°58′9.4″	N.A.	13OULI-A	11.4	149	3	1.8	0.02	1.8	0.01	0.7	0.0	0.7	0.1
				13OULI-B	8.6	120	2	1.9	0.03	1.9	0.02	0.5	0.0	0.6	0.1
				13OULI-C	9.1	129	3	1.8	0.03	1.8	0.02	0.6	0.0	0.7	0.1
Breccia [5]	Euhedral goethite close to quartz and K-feldspars	N 37°01′33.0″; E 9°06′13.0″	Unknown for pure goethite. Isotopic values contaminated by quartz and feldspars	140B-02-A	7.3	547	11	6.7	1.08	7.0	0.16	0.7	0.0	0.7	0.1
				140B-02-B	12.7	359	7	2.8	0.34	2.9	0.12	1.0	0.1	1.1	0.1
				140B-02-C	9.2	332	7	4.7	0.86	4.9	0.18	0.6	0.0	0.6	0.1

* nccSTP = nano cubic-centimeters-at-standard-temperature-and-pressure; ** error at 1 sigma; *** eU = effective uranium.

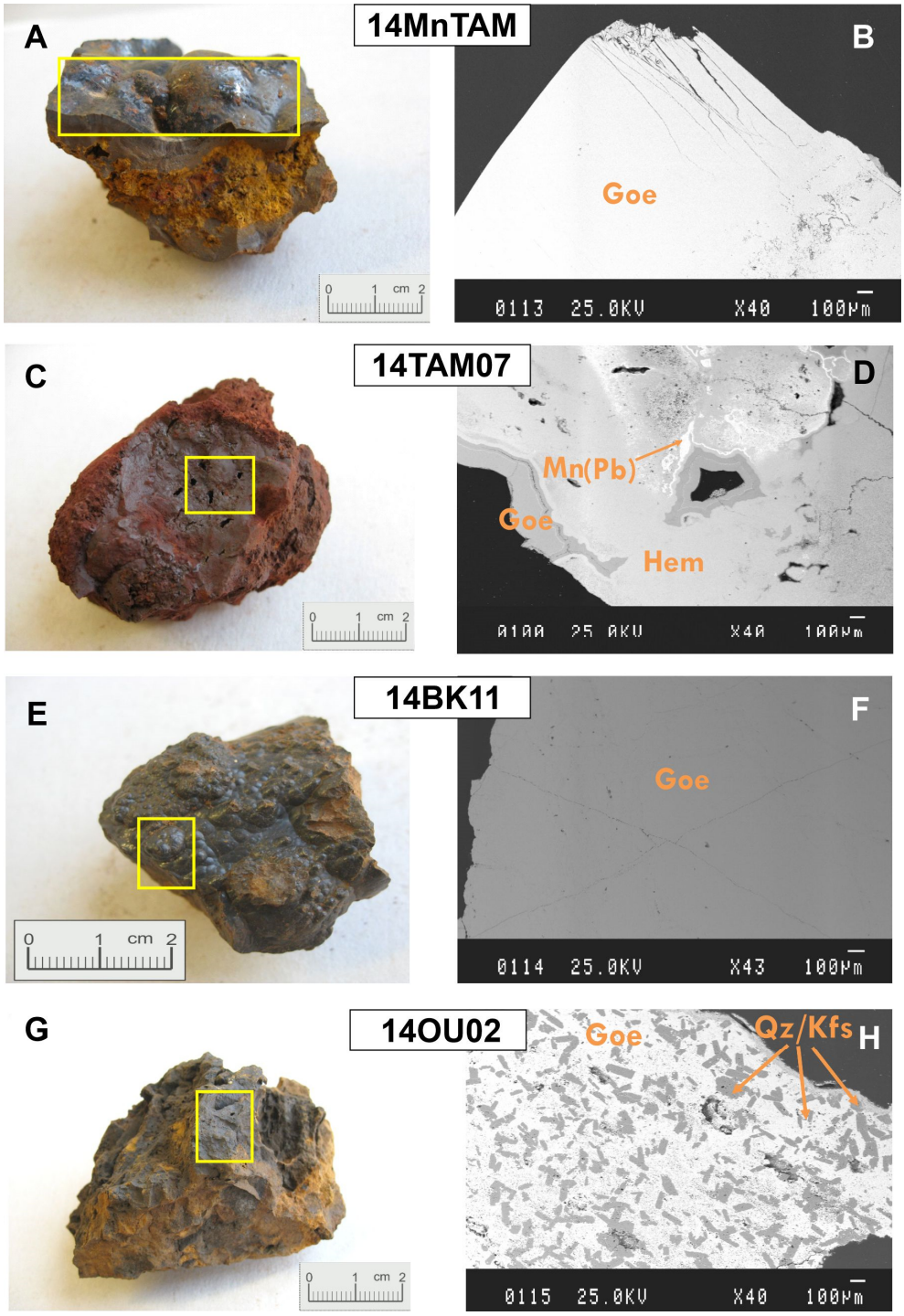

Figure 3. Samples of studied goethite and SEM microphotograph in back-scattered electrons mode, showing the pure character of supergene goethite of the samples 14MnTAM and 14BK11. Goe = goethite; Hem = hematite; Qz = quartz; Kfs = K-feldspar. (**A**) sample 14MnTAM, (**B**) SEM microphotograph in back-scattered electrons mode of sample 14MnTAM, (**C**) sample 14TAM07, (**D**) SEM microphotograph in back-scattered electrons mode of sample 14TAM07, (**E**) sample14BK11, (**F**) SEM microphotograph in back-scattered electrons mode of sample 14BK11, (**G**) sample 14OU02, (**H**) SEM microphotograph in back-scattered electrons mode of sample 14OU02.

The mineralogy of samples was characterized using an X-ray Panalytical X'Pert Pro (Malvern Panalytical Ltd., Palaiseau, Essone, France) and a diffractometer Philips PW3710 (Philips, Amsterdam, Holland, the Netherlands) (CuKα radiation), and a JEOL 7500 (Jeol

Ltd., Akashima, Tokyo, Japan) scanning electron microscope (SEM) coupled to an energy dispersive electron spectrometer (EDS).

The (U-Th)/He dating method relies on the ^{4}He production, ejection, and accumulation inside the crystal structure during alpha decay of the radioactive U-Th chains [21]. The (U-Th)/He age is determined by measuring the total He content of the samples and in a second step, the total U and Th content. (U-Th)/He ages were obtained in the GEOPS laboratory (University Paris-Saclay, Orsay, France) for three aliquots per sample, except for 14BK11 where only two aliquots were analyzed. For samples composed of several iron (oxyhydr-)oxide generations, the purest zones were selected to avoid erroneous and meaningless ages. First, fragments manually extracted from the hand-sized samples were cleaned using an ultrasonic bath and rinsed with milli-Q water and ethanol. Aliquots were handpicked under a binocular microscope, weighed, and encapsulated into niobium envelopes (purity 99.9%). Fragments with a length exceeding 0.5 mm and a weight around 0.5 mg for 14OU03 sample and ranging between 6 and 18 mg for other samples were selected. Each encapsulated sample was degassed using a diode Ytterbium laser under vacuum for thirty minutes at temperatures below 1000 °C. This procedure was repeated until all ^{4}He was degassed. The ^{4}He gas was mixed in the purification line with a known amount of ^{3}He, and purified. Helium isotopes (^{3}He and ^{4}He) were measured with a Pfeiffer Prisma Quadrupole mass spectrometer to ensure the purity of the analytical gas (see reference [22] for more details). After degassing, samples were extruded from the envelopes directly into 5 mL Teflon-capped vials for complete dissolution. Firstly, 100 µL of 5 M HNO_3 containing a known amount of ^{230}Th and ^{235}U was introduced in each vial followed by 400 µL of 30% HCl, and a few drops of 38% HF. Vials were closed and heated up to 100 °C overnight. Solutions were evaporated at 100 °C to concentrate the sample. If samples were not completely dissolved, the procedure of adding HCl and HF was repeated. Secondly, 5 mL of 5 M HNO_3 was added and heated for one hour at 100 °C. The solution was diluted with 1 M HNO_3 to set the iron content at 100 ppm. The U and Th measurements were undertaken by using a quadrupole ICP-QMS series^{II} CCT Thermo-Electron at LSCE (Laboratoire des Sciences du Climat et de l'Environnement—Gif sur Yvette, France). The analytical error for He and U-Th measurements is 5% at 1σ.

The fossil specimens illustrated here, collected by local miners in 1934 at the Douahria Fe deposit, are stored in the Paleontological Collection of the University Lyon 1-Villeurbanne (FSL).

4. Results

Table 1 shows the (U-Th)/He data obtained on goethite collected in the Nefza-Sejnane district. Most of the prepared samples are pure goethite. Two samples (14TAM07 and 13NEFZA) are made of a mixture of goethite with other phases such as hematite and a Mn-Pb oxide (see Figure 3D). Another sample (14OU02) is composed of a mixture of goethite, quartz, and K-feldspar (Figure 3H). All samples present relatively homogeneous, effective uranium (eU = U + 0.24Th) contents ranging from 0.5 to 7 ppm. In addition, most samples have quite similar Th/U ratios around 0.01–0.2. Only one sample is characterized by a significantly higher Th/U ratio of 1.7 ± 0.1 (14TAM07, Table 1). The variability in the Th/U ratio, which may be used to trace differences in the iron oxide populations or the presence of inclusions [23,24], confirms the relatively high content of hematite in sample 14TAM07. The raw (U-Th)/He ages range from 0.5 ± 0.03 to 8.1 ± 0.4 Ma and are mostly homogeneous per sample. No correction of alpha ejection has been considered here, because the mean alpha stopping distance of the ejected He in iron oxides and hydroxides ranges from 14 to 16 µm [25]. These values are small compared to the sample's size (~0.5 mm). On the other hand, as He can be lost by diffusion due to the polycrystalline nature of the samples (see reference [26] for a review), He losses are corrected by applying a 10% correction on the He age and a 10% error (Table 1). For example, Schuster et al. (2005) and Monteiro et al. (2014) applied a 5% to 30% correction for goethite (U-Th)/He ages based on diffusion data measured directly on the dated crystals [23,27]. In this study, we used a 10% correction

on the raw ages and applied an additional error of 10%, allowing to estimate He losses by diffusion, which represents the sum of the analytical error and the error on the He diffusion loss estimation, similarly to reference [22] (Table 1). This correction will not significantly change the age interpretation but will be used in the following discussion since it better reflects crystallization ages. The reproducibility of He ages obtained for Tamra and Boukchiba goethite is better than the 10% error estimated to account for He diffusion processes, which gives good confidence in the present data. However, a 10% error is preferred to take into account a potential He diffusion. With this He correction, the oldest episode, at about 8.5 Ma, is recorded in Tamra and Boukchiba. The latest episode, younger than ca. 1 Ma, is recorded in Ouchtata, Oued Belif, and Tamra (Table 1). In summary, most of the present (U-Th)/He ages are reproducible (Table 1), highlighting two main episodes of supergene goethite formation, with mean ages at 8.6 ± 0.9 Ma and 0.8 ± 0.2 Ma (Table 1 and Figure 4).

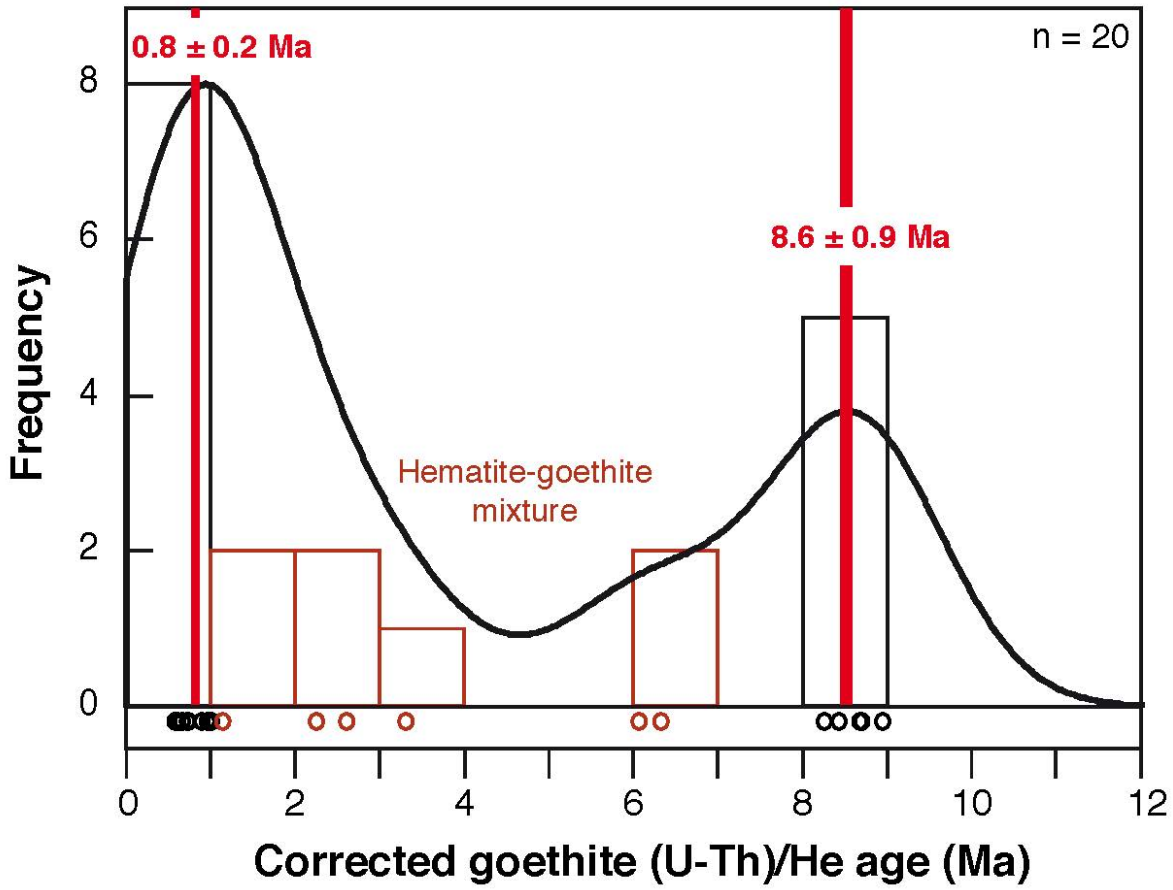

Figure 4. Corrected (U-Th)/He histogram age: supergene goethite in black histogram boxes and black circles (our data); hematite-goethite mixture in brown histogram boxes and brown circles (our data). The two main crystallization phases of supergene goethite at 8.6 ± 0.9 Ma and 0.8 ± 0.2 Ma are also reported in red. For hematite-goethite mixed samples, (U-Th)/He ages range between the two main weathering phases.

5. Discussion

5.1. (U-Th)/He Age Significance Using Petrographic Examination of Goethite

Most of the studied samples show pure and well-crystallized supergene goethite, allowing us to obtain, for the first time in Tunisia, direct robust dating of two episodes of major meteoric fluid circulation at 8.6 ± 0.9 Ma and 0.8 ± 0.2 Ma. The ages between these two main episodes reflect the mixture of goethite with other mineral phases. The 14TAM07 sample clearly shows a mixture of goethite and hematite, with several phases of crystallization and potential contamination by Mn-Fe phases (Figure 3D). This mixture

most likely explains the large variation observed in (U-Th)/He ages, from 3.3 ± 0.3 Ma to 6.3 ± 0.6 Ma, in between the two main episodes (~8.6 and ~0.8 Ma). A similar interpretation is proposed for the 13NEFZA sample, with (U-Th)/He ages ranging from 1.0 ± 0.1 Ma to 2.6 ± 0.3 Ma. The sample 14OB02, which is made of goethite, quartz, and K-feldspar, provides (U-Th)/He ages (0.6 ± 0.1 to 1.1 ± 0.1 Ma) that overlap with the other samples. This suggests that (U-Th)/He method is not affected by potential mixing of goethite with quartz and K-feldspars, the latter typically having a relatively poor content in U, Th, Sm, He compared to goethite.

5.2. Age of the Meteoric Fe-Fluids Circulation in the Nefza-Sejnane District

The new (U-Th)/He data highlight two episodes of Fe-rich meteoric fluids circulation in the Nefza-Sejnane district, at 8.6 ± 0.9 Ma and 0.8 ± 0.2 Ma.

5.2.1. Late Tortonian Weathering Event (8.6 ± 0.9 Ma)

The oldest (U-Th)/He ages (mean age of 8.6 ± 0.9 Ma) are obtained on goethite samples from the Tamra and Boukchiba localities. The Tamra Formation, deposited during a regional extensional tectonic regime [13], consists of successive sedimentary sequences [2]. Each sedimentary sequence results from (1) sedimentation of iron-rich inherited material, and (2) in situ pedogenesis and iron concentration without evidence of a precursor hydrothermal event. This clearly confirms that Fe-(oxi)hydroxide formation resulted (at least partly) from the involvement of meteoric fluids in the area. In this context, extensional regime has provided the geological drains (fractures, faults, . . .), allowing the fluids to percolate within sediments, as it has been previously suggested for numerous weathering profiles in various areas (e.g., [28,29]). The 14MnTAM sample, showing GHe ages between 8.9 ± 0.9 Ma and 8.4 ± 0.8 Ma (Table 1), is clearly related to weathering, as suggested by (i) its botryoidal texture (Figure 3A) and (ii) the δD and $\delta^{18}O$ data highlighting its formation in equilibrium with meteoric waters [4]. This relatively old age may also be associated with pedogenesis recognized during the deposition of the sequence [2]. This episode of weathering is likewise recognized at Boukchiba, where the GHe ages of 14BK11 range from 8.7 ± 0.9 Ma to 8.2 ± 0.8 Ma, which are consistent with those of the sample 14MnTAM. Sediments at Boukchiba also experienced weathering, as attested by the δD and $\delta^{18}O$ data obtained onto the same sample of goethite. These data suggest that goethite formed in equilibrium with meteoric waters during late Tortonian period, but was not affected by synsedimentary pedogenesis of the subaerial Tamra Formation [5]. The sample 14BK11 (Figure 3E,F), which is made of pure goethite, is located in a vein cross-cutting the Oued Belif breccia and associated to Fe-LREE-U mineralization. Then, the late Tortonian weathering period is recorded in the synsedimentary pedogenesis of the Tamra Formation (sample 14MnTAM) and in the surrounding brecciated rocks, suggesting at least a local event of weathering.

5.2.2. Late Pleistocene Weathering Event (0.8 ± 0.2 Ma)

The 14OU03, 13OULI, and 14OB02 samples, located in various localities in the district (see Figure 2 and Table 1), present consistent GHe ages, ranging from 1.0 ± 0.1 Ma to 0.6 ± 0.1 Ma. These ages highlight meteoric Fe-rich fluid circulation during a late episode around 0.8 ± 0.2 Ma in the Nefza-Sejnane district.

5.3. Stratigraphic Frame of the Nefza-Sejnane District

These new (U-Th)/He ages allow refining the stratigraphic frame of the Nefza-Sejnane district, especially from Tortonian to Pleistocene times (Figure 5).

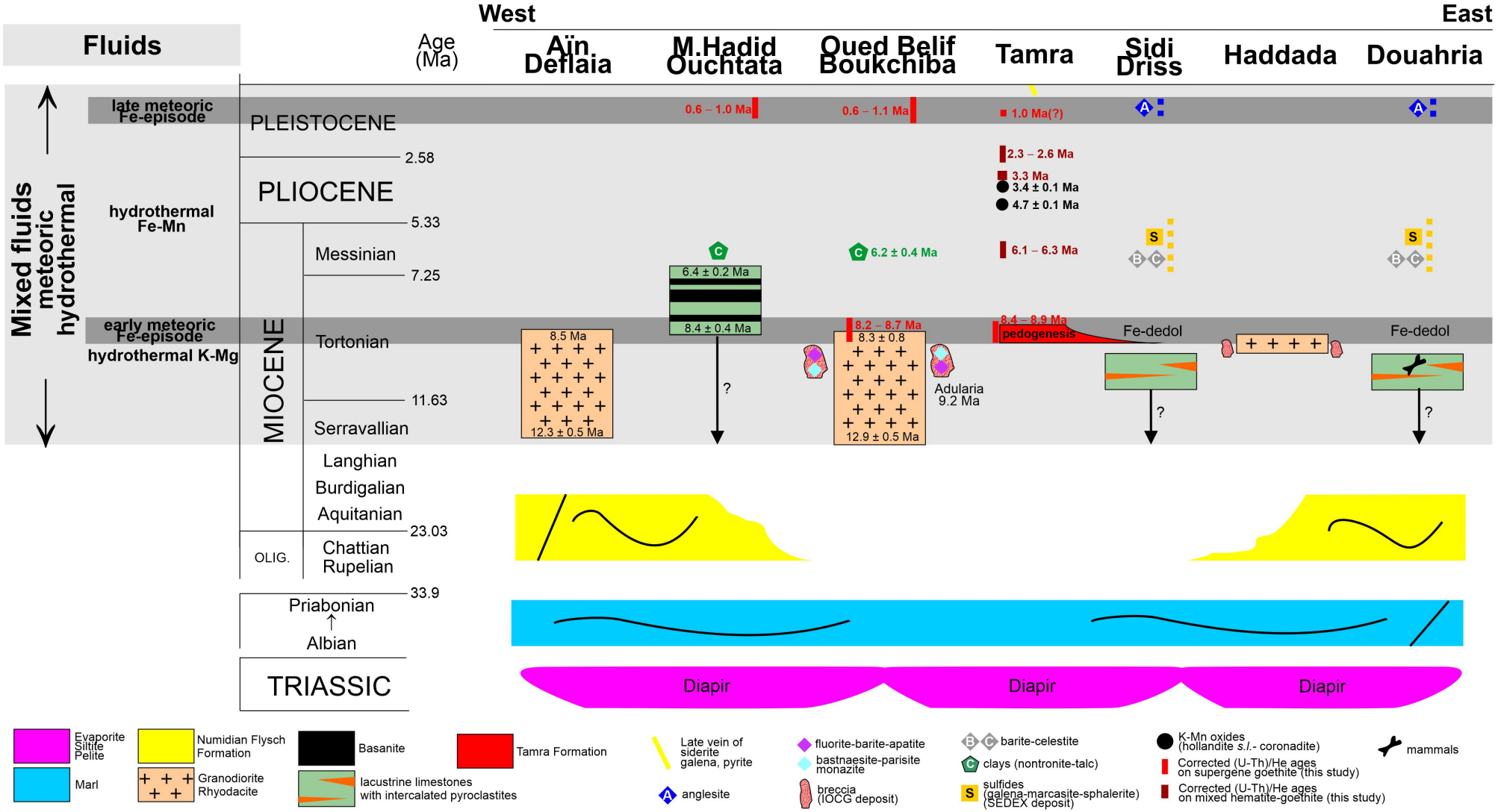

Figure 5. Stratigraphic frame of the Nefza-Sejnane district (Tunisia), including the new (U-Th)/He data on Fe (oxyhydr-)oxides. In red: data on supergene goethite; in red purple: data on mixed hydrothermal-meteoric hematite-goethite. Olig. = Oligocene. Questions marks (?) refer to potential larger stratigraphic extension.

The entire nappe pile that forms a large part of the regional substratum is cut by shallow-level, Serravallian to lower Tortonian intrusive rocks. The felsic rocks of the whole district are dated between 12.9 ± 0.2 Ma and 8.2 ± 0.4 Ma (see a detailed review in reference [14]). In the Zouara basin (Figure 2), the transitional basalt sills exposed at Mokta el-Hadid have been dated at 8.4 ± 0.4 Ma [30], and at 6.9 ± 0.3 and 6.4 ± 0.2 Ma [17]. Some of these ages are discussed/questioned by Decrée et al., 2016 [14]. Anyway, the widespread middle-late Miocene bimodal magmatism is largely recognized at the scale of the whole district.

The age of the Tamra Formation was not precisely known but was supposedly Miocene–Pliocene or younger according to the 1:50,000 geological map of Nefza [16,17]. Our new dating refines the age of the Tamra succession. The deposition of the Tamra sediments is globally coeval with the oldest GHe age associated with the synsedimentary pedogenesis, at 8.6 ± 0.9 Ma. This suggests that the Tamra Formation is late Tortonian in age. At the time, meteoric waters may have played a role in the formation of halloysite and kaolinite and/or destabilization of primary clays in the Tamra ore. However, these meteoric fluids would have been mixed at some stage with deep hot saline fluids related to a thermally-driven circulation [4]. It confirms that the Tamra Formation experienced polyphased and mixed hydrothermal/meteoric fluid circulations, as already stressed by Decrée et al., 2008b [2].

The Tamra iron-stained sediments overlay the Sidi Driss sediments (Figure 5). The latter can be correlated with the Douahria sediments, based on (i) regional lithological similarities; (ii) the presence of volcanoclastic intercalations in the Douahria and Sidi Driss sequences, including cinerites [1,9]; and (iii) their similar gastropod fauna [31,32]. The Sidi Driss and Douahria sediments were attributed to the late Miocene (Messinian?) by reference [1]. Our data suggest a minimum Tortonian age for these sediments, close to or at the end of the magmatic activity in the area (Figure 5). This is in good agreement with the isotopic results [9], demonstrating that the metals in the Nefza-Sejnane deposits were supplied by the regional magmatic through hydrothermal fluids. Interestingly, Decrée et al. [2] observed that the Sidi Driss and Douahria sulfide ore deposits are hosted within carbonate lenses initially composed of Fe–Mn-enriched dedolomite. The dedolomitization is a well-known process that usually takes place when dolomite interacts with meteoric fluids (e.g., [33]). Concurrently with an Mg loss, a Fe–Mn gain led to formation of Fe–Mn carbonates or pure calcite (in the absence of Fe–Mn gain). At Sidi Driss and Douahria, dedolomitization is observed in the first stage of the ore sequence, before the early replacement by barite and celestite [1]. Consequently, dedolomitization could be related to the late Tortonian episode of weathering recognized at Tamra (Figure 5).

In the Nefza-Sejnane district, the late Tortonian episode of weathering was followed by circulation(s) of hydrothermal fluids, leading to the precipitation of nontronite and talc observed in several localities of the district and dated at 6.2 ± 0.4 Ma [34]. Neoformation of nontronite and talc is observed mainly in (i) the basaltic flows of Mokhta El Hadid (Zouara basin); and (ii) the Triassic material and Miocene rhyodacite of Oued Belif (Figures 2 and 5). These hydrothermal circulations are most likely involved in the mineralization in Pb-Zn sulfides, barite, celestite, and fluorite at Sidi Driss and Douahria. Mn oxides constitute another milestone for the district. Decrée et al. [2] stressed that hydrothermal enrichment was superimposed on the weathering conditions found in the Tamra sequence, leading to the formation of first, hollandite, romanechite, and Sr-cryptomelane, dated at 4.7 ± 0.1 Ma by ^{40}Ar-^{39}Ar dating, and then coronadite, chalcophanite, and amorphous Mn-oxides at 3.4 ± 0.1 Ma. Hydrothermal circulations were confirmed by Dekoninck et al. [4], studying the δD and δ^{18}O isotopes of kaolinite-halloysite not in equilibrium with meteoric waters. Our new data show that a late Tortonian weathering phase predates the Messinian–Pliocene hydrothermal episodes leading to the formation of Mn oxides, Pb-Zn sulfides, barite, celestite, and fluorite.

A late Pleistocene weathering episode has been established by our new (U-Th)/He analyses. This recent meteoric fluid circulation is most probably responsible for the late

occurrence of anglesite and iron oxide at Sidi Driss and Douahria [1]. The meteoric fluids associated with this recent weathering event affected the whole district. They are most likely responsible for the numerous weathering profiles observed in the area, including in the superficial part of the Albian–Priabonian marls and in the Numidian Flysch Formation, which hosts kaolinitic industrial clays [3,6,7].

5.4. Significance of the Weathering Episodes at a Regional Scale

The suitable conditions for the development of significant weathering profiles generally result from a combination of slow large-scale tectonic movement and (sub)tropical climate. At a regional scale, the new ages obtained contribute to unravel the role of (i) the geodynamic/tectonic setting, since exposure to weathering depends on exhumation (uplift) creating a hydrodynamic gradient for the percolation of meteoric fluids, and (ii) the climate, considering that meteoric water/fluid is needed. Our new data highlight two episodes of weathering, during the late Tortonian and the late Pleistocene, in the Nefza-Sejnane district. Interestingly, weathering events were already known during these periods in Tunisia. Based on C-O stable isotopes of non-sulfide Zn-Pb Tunisian deposits, Garnit et al. [35] suggested that Tunisian supergene deposits resulted from weathering during the middle to late Miocene interval and the Pliocene-Quaternary period. Studying the karstic system in Aïn Khamouda (Central Tunisia), Bruyère et al. [36] concluded that karstification took place in Tortonian or post-Tortonian period, as for other comparable karsts located in the Algerian Constantinois. Our new (U-Th)/He data on goethite refine the previously suggested episodes of weathering in Tunisia.

Climate has been regarded as an important parameter of weathering periods because sufficient water supply is needed for weathering processes (e.g., [37]). Beauvais and Chardon [38] and Chardon et al. [39] in West Africa propose that long-term eustatic sea level fall and climate play a significant role in weathering profiles. The late Pleistocene is marked by wet climate in North Africa ("African Humid Period"; e.g., [40]). Tortonian climate was presumably humid to subhumid around the Mediterranean Sea, while the hinterland was dryer ([41–43]), as is the case today. During the late Tortonian, North Africa experienced a temporary turnover from dry to wet climate, initiating the "Zeit Wet Phase" of the Messinian (e.g., [44]). Conversely, our GHe ages do not match Cenozoic warmest climates in the studied area. Comparing these climatic conditions with the weathering periods obtained by our new data supports that warm climate is a second-order control, whereby wet climatic conditions are necessary to ensure the existence of meteoric fluids. The relatively high precipitation during the late Tortonian and late Pleistocene provided water to the weathering system, when differential uplift movements generated the weathering gradient for the downward migration of meteoric fluids.

Large-scale, vertical, positive movements were able to produce protore (including potential hypogene sulfides) uncapping and weathering, by creating a gradient for the percolation of meteoric fluids. In the last decade, the temporal link between uplift-related exhumation and weathering periods at a regional scale has been documented by several studies, in various geological contexts. Using ^{40}Ar-^{39}Ar method on cryptomelane in Mn ores of Democratic Republic of Congo, De Putter et al. [28], Fontaine et al. [45] and De Putter and Ruffet [46] highlighted successive episodes of weathering since Late Cretaceous and concluded that tectonics accounts for most of the recognized supergene ore formation episodes, which are controlled by vertical lithospheric movements that are ultimately responsible for alternating stages of landscape stability and erosion. In the Ardenne (Western Europe), a recent synthesis showed that the uplift of the area was most probably the main factor triggering the development of weathering mantles, together with the increasing seasonality and high precipitation [47], illustrating the role of geodynamics and climate in the weathering.

In the same way, our results may be interpreted in relation with the regional Mediterranean geodynamics. In Morocco, weathering episodes are most likely associated with some of the four main Atlasic geodynamic events, as attested in recent geodynamic and ore

deposits studies [48–50]. In Tunisia, both periods of weathering highlighted by our new (U-Th)/He data correspond to two distinct Alpine tectonic pulses that produced the exhumation of sulfides ores [35]. Alpine compressional movements may have caused marked slow and large-scale (at least regional) uplifts, preventing deposition of coeval sediments, except in the local extensional basin, such as in Tamra and Zouara basins. Then, the studied area must be regarded as an elevated zone during late Tortonian and late Pleistocene times, favoring the formation of weathering profiles. In the Iberian Pyrite Belt (Southern Spain), preliminary ages of different parts of the gossans using ^{40}Ar-^{39}Ar techniques show that at least two stages of oxidation took place at 7–8 Ma and about 1–2 Ma [51], quite coeval with the new GHe ages in Tunisia. The late Tortonian meteoric episode corresponds to a turning point in Mediterranean basin dynamics with the disruption of the Mediterranean–Atlantic connection, an important tectonic rearrangement due to rollback of the Gibraltar slab [52,53]. This may suggest that the late Tortonian and late Pleistocene time intervals are periods of weathering at the Mediterranean region scale, partly driven by (at least regional) large-scale uplift-related exhumation associated to Alpine events. Further studies in the Atlasic and Mediterranean domains are, however, required to refine the nature, scale, and role of this uplift-related weathering, assuming the available age record is complete.

5.5. Revision and Refined Age of the Mammalian Fauna in the Douahria Fe-Deposit

Our new GHe ages refine the stratigraphy of classic fossils from the Douahria Fe-deposit (known as Douaria in most paleontological works). The fossils comprise two land snail species (*Helix* (*Iberus*) *fossulata* and *Helix* (*Archelix*) *solignaci*; [11–18]) and large mammal remains. The latter elements were discovered by local miners in 1934, in a ferruginous crust of the Fe-rich deposit at Douahria ([11]; Figure 2). The vertebrate remains were then assigned to taxa of both eastern Mediterranean (the rhinocerotid "*Rhinoceros pachygnathus*" (= *Ceratotherium neumayri* [54] sensu [55]) and the giraffid "*Helladotherium duvernoyi*" and Asian affinities (the anthracotheriid "*Merycopotamus dissimilis*"), further indicating a latest Miocene age). Historically, this paleontological assemblage provided the first argument for assigning a late Neogene age to the Nefza-Sejnane ore deposits [11]. The taxonomic assignment of the rhinocerotid was later revised by Guérin [18], who named the new species *Diceros douariensis* after the remains from Douahria.

The stratified Fe ore of Douahria is stratigraphically correlated with the SEDEX-type Pb-Zn ore of Sidi Driss related to thermally-driven fluid circulations [1]. From biostratigraphic and biogeographic perspectives, the Douahria gastropod assemblage has a late Neogene signature at a Maghreb scale (late Miocene–Pliocene; [31,32]), without further precision. Only a late Miocene age of these fossils is in agreement with our (U-Th)/He dating of the Fe-rich fluids (ferruginous crust) of the area, suggesting that the first episode of ferruginous crust containing the fossils is late Tortonian in age (8.6 $\pm$ 0.9 Ma—see above).

A systematic revision of the mammalian fauna from Douahria may provide a better age constraint. The giraffid from Douahria was first referred to as "*Helladotherium duvernoyi*", a short-necked sivatheriine species originally described by Gaudry and Lartet [56] at Pikermi, a classic late Miocene vertebrate locality from Greece (dated around the Tortonian–Messinian transition, at 7.5–7 Ma; for review, see [57]). The dental and postcranial remains were recently reassigned to the longer-ranged sivatheriine *Sivatherium hendeyi* [57], documenting the late Miocene–early Pliocene interval in Africa (11.6–4 Ma; [20,58]). The Douahria anthracotheriid was originally assigned by Roman and Solignac [11] to the Asian species "*Merycopotamus dissimilis*", of late Miocene–earliest Pleistocene range (7.8–2.4 Ma [59]). In their revision of African anthracotheriids, Holroyd et al. [60] and Lihoreau et al. [61] consider that the referred specimens from Africa belong to *Libycosaurus* instead. Dental features and moderate dimensions further closely match those of *Libycosaurus anisae* [62], known to range the latest middle–early late Miocene interval in East and North Africa (~12–10 Ma [60,61]). Aside from Douahria, this species has been recognized in Central Tunisia (Bled Douarah, Beglia Formation, early late Miocene [61]) and Southern Tunisia (El Ziz, late Miocene [63]). The two-horned rhinocerotine rhinocerotid

Diceros douariensis was named by Guérin [18] based on the abundant craniomandibular and postcranial material from Douahria. Guérin [64] proposed an age of 9.5 Ma for the latter locality, based on biostratigraphic correlations with the Djebel Krechel el Artsouma (Central Tunisia) and other circum-Mediterranean occurrences of *D. douariensis*. Geraads [19] later reassigned this species to *Ceratotherium* and considered that specimens from As Sahabi, Northern Libya (latest Miocene; 6.2–5.33 Ma) were also probably assignable to *Ceratotherium douariense*, thus significantly extending upward its stratigraphic range (i.e., 9.5–5.33 Ma). From a morpho-anatomical perspective, this species has the closest affinities with *Ceratotherium neumayri* [54], a conspicuous element of eastern Mediterranean faunas throughout the late Miocene (e.g., [55,65]).

Direct re-examination of the specimens in the Lyon University collection led to the unexpected recognition of a second rhinocerotid taxon at Douahria, as already mentioned by Geraads [19]. Most rhinocerotid remains do belong to *C. douariense*, as typified by the adult skull FSL 16749 (holotype; Figure 6A,B). Nevertheless, the juvenile skull FSL 16752 (Figure 6C–F), previously defined as the paratype of "*Diceros douariensis* Guérin, 1966", has cranial and dental characteristics discarding any referral to a two-horned rhinocerotine, such as the presence of a concave dorsal profile and a rounded nasal notch (Figure 6C), of laterally-projected orbits (Figure 6D), of a lingual wall on upper premolars (Figure 6E), of sagittally-elongated molars with an ectoloph undulated in occlusal view, and the abundance of cement filling the valleys of cheek teeth (Figure 6F). These features are diagnosing middle and early late Miocene elasmotheriine rhinocerotids from Eurasia and Africa, i.e., the ones retaining non-ever-growing teeth [66–68]. The juvenile skull FSL 16752 cannot be assigned to any known elasmotheriine species, notably as documented in Africa (i.e., *Kenyatherium bishopi* [69]; *Ougandatherium napakense* [70]; *Victoriaceros kenyensis* [71]; *Samburuceros ishidai* [68]; and references therein). It is most likely documenting a new species, the formal description of which is far beyond the scope of the current work. Accordingly, no precise biostratigraphical age can be formally inferred from this occurrence, as usual regarding new taxa. Yet, given its evolutionary stage among elasmotheriine rhinocerotids [66,67], a late middle to early late Miocene age can be suspected for the first appearance of this taxon. Independently, the Douahria assemblage can be refined at ~11.6–10 Ma, thanks to the concurrent range of the bothriodontine anthracotheriid *Libycosaurus anisae* [62] and of the sivatheriine giraffid *Sivatherium hendeyi* [20] documenting the 12–10 and 11.6–4 Ma interval, respectively (Figure 7). This stratigraphical range as inferred for Douahria is further compatible with its rhinocerotid components. A Tortonian age is thus supported here for the Douahria mammalian assemblage. Accordingly, deposition of the Douahria fossils may have occurred in (early) Tortonian times, just prior to the circulation of the meteoric fluids, here dated late Tortonian (8.6 $\pm$ 0.9 Ma) by (U-Th)/He method (Figure 7). No long gap is necessarily to be suspected between both the events.

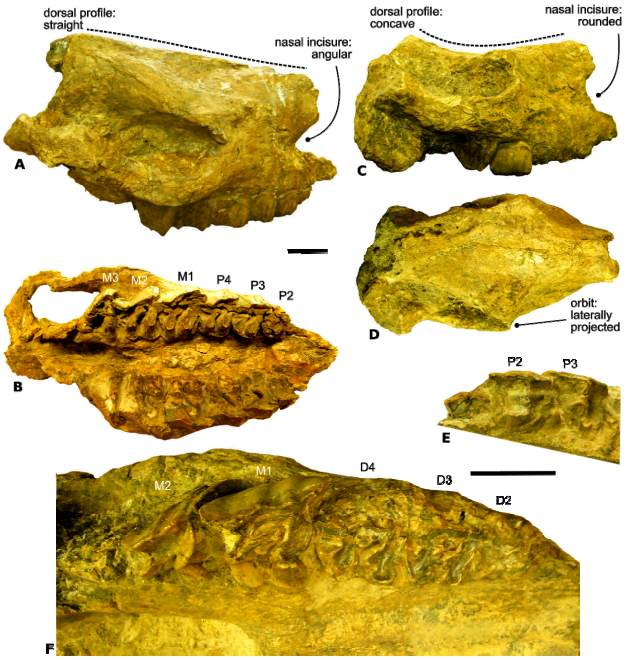

Figure 6. Selected rhinocerotid remains from the early Tortonian Douahria fossil locality, Tunisia. (**A**,**B**), *Ceratotherium douariense* [19], adult skull FSL 16749 (holotype). (**A**), right lateral view; (**B**), palatine view, with left and right dental series (premolars (P2–P4) and molars (M1–M3)). (**C**–**F**), Unidentified elasmotheriine, juvenile skull FSL 16752 (formerly paratype of *C. douariense*). (**C**), right lateral view; (**D**), dorsal view; (**E**), detailed occlusal view of the left dental series, with emerging 2nd and 3rd premolars (P2–P3); (**F**), detailed occlusal view of the right dental series, with decidual teeth (D2–D4) and functional 1st and 2nd permanent molars (M1–M2). Scale bars = 5 cm.

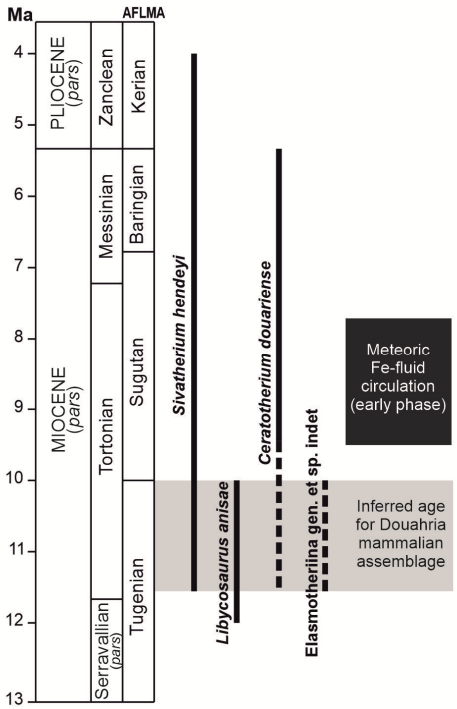

Figure 7. Biochronological chart of late Neogene times, detailing the inferred ages of both the Douahria mammalian assemblage and first phase of meteoric fluid circulation. Biochronological data from [19,20,60,61]. AFLMA = African Land Mammal Ages [72].

6. Conclusions

The new (U-Th)/He ages obtained on goethite in the mineralized and vertebrate-bearing sediments of the Nefza-Sejnane district (Tunisia) highlight that:

- meteoric fluids circulated during late Tortonian (8.6 ± 0.9 Ma) and late Pleistocene (0.8 ± 0.2 Ma) time intervals, confirming the polyphased and mixed (hydrothermal/meteoric) fluid circulations in the district and their role in the genesis of part of the mineralization,
- these events allow refining the ages previously suggested for weathering episodes in Tunisia, confirming that (U-Th)/He on rigorously sampled and well-characterized (using petrography and δD-$\delta^{18}O$ analyses) goethite is a very powerful method to decipher weathering periods,
- these episodes are coeval with geodynamic events and wet climates in North Africa, confirming a temporal link between weathering events and both regional tectonics and humid periods, as already stressed by other studies in other areas,
- matched with previous stratigraphic data, the chronological frame of the district is refined, allowing the integration of the numerous regional deposits (Pb, Zn, Fe, Mn, LREE, U, clays),
- consequently, the deposition of the Douahria fossils in a ferruginous crust, here taxonomically revisited, occurred no longer prior to the late Tortonian circulation of the meteoric Fe-fluids, here dated by (U-Th)/He method.

Author Contributions: Conceptualization, J.Y.; data curation, C.G.; formal analysis, M.V., B.M. and S.D.; funding acquisition, J.Y. and F.J.; investigation, J.Y., M.V., P.-O.A., B.M., A.D., S.D., H.-R.C., N.H. and C.D.; methodology, M.V., C.G. and R.P.-J.; project administration, J.Y.; software, C.G.; supervision, J.Y. and F.J.; writing—original draft, J.Y., M.V., C.G., P.-O.A., A.D. and S.D.; writing—review and editing, J.Y., A.D. and P.-O.A. All authors have read and agreed to the published version of the manuscript.

Funding: Wallonie-Bruxelles International: Projet 8-axe 2 Agence Nationale de la Recherche: RECA ANR-17-CE01-0012-01.

Institutional Review Board Statement: Not applicable.

Informed Consent Statement: Not applicable.

Data Availability Statement: Not applicable.

Acknowledgments: P.-O.A. is particularly grateful to Emmanuel Robert (Université de Lyon; Douahria specimens) and to Christine Argot (Muséum National d'Histoire Naturelle, Paris; comparison material) for having granted access to the collections they are in charge of, and to Fabrice Lihoreau and Denis Geraads for sharing their expertise. This work was partly funded by the Belgian Science Policy Office, project BR/121/A3/PALEURAFRICA, and by the project entitled "Valorisation des argiles tunisiennes" of WBI (Wallonie-Bruxelles International). This research used resources of the Electron Microscopy Service, which is a member of the "Plateforme Technologique Morphologie–Imagerie" of the University of Namur (UNamur). Michèle Verhaert thanks the Belgian National Fund for Scientific Research (FNRS), for providing a FRIA PhD grant. C.G. thanks the RECA ANR-17-CE01-0012-01 project for funded (U-Th)/He analysis.

Conflicts of Interest: The authors declare no conflict of interest.

References

1. Decrée, S.; De Putter, T.; Yans, J.; Moussi, B.; Recourt, P.; Jamoussi, F.; Bruyère, D.; Dupuis, C. Iron mineralisation in Mio-Pliocene sediments of the Tamra iron mine (Nefza mining district, Tunisia): Mixed influence of pedogenesis and hydrothermal alteration. *Ore Geol. Rev.* **2008**, *33*, 397–410. [CrossRef]
2. Decrée, S.; Ruffet, G.; De Putter, T.; Baele, J.-M.; Recourt, P.; Jamoussi, F.; Yans, J. Mn oxides as efficient traps for metal pollutants in a polyphase low-temperature Pliocene environment: A case study in the Tamra iron mine, Nefza mining district, Tunisia. *J. Afr. Earth Sci.* **2010**, *57*, 249–261. [CrossRef]
3. Moussi, B.; Medhioub, M.; Hatira, N.; Yans, J.; Hajjaji, W.; Rocha, F.; Labrincha, J.A.; Jamoussi, F. Identification and use of white clayey deposits from the area of Tamra (northern Tunisia) as ceramic raw materials. *Clay Miner.* **2011**, *46*, 165–175. [CrossRef]

4. Dekoninck, A.; Moussi, B.; Vennemann, T.; Jamoussi, F.; Mattielli, N.; Decrée, S.; Chaftar, H.-R.; Hatira, N.; Yans, J. Mixed hydrothermal and meteoric fluids evidenced by unusual H- and O-isotope compositions of kaolinite-halloysite in the Fe(-Mn) Tamra deposit (Nefza district, NW Tunisia). *Appl. Clay Sci.* **2018**, *163*, 33–45. [CrossRef]
5. Decrée, S.; Marignac, C.; De Putter, T.; Yans, J.; Clauer, N.; Dermech, M.; Aloui, K.; Baele, J.-M. The Oued Belif Hematite-Rich Breccia: A Miocene iron oxide Cu-Au-(UREE) deposit in the Nefza Mining District, Tunisia. *Econ. Geol.* **2013**, *108*, 1425–1457. [CrossRef]
6. Chargui, H.; Hajjaji, W.; Wouters, J.; Yans, J.; Jamoussi, F. Orange Selophenyl TGL dye fixation by modified kaolin. *Clay Miner.* **2018**, *53*, 271–287. [CrossRef]
7. Moussi, B.; Hajjaji, W.; Hachani, M.; Hatira, N.; Labrincha, J.-A.; Yans, J.; Jamoussi, F. Numidian clay deposits as raw material for ceramics tile manufacturing. *J. Afr. Earth Sci.* **2020**, *164*, 103775. [CrossRef]
8. Jallouli, C.; Mickus, K.; Turki, M.M.; Rihane, C. Gravity and aeromagnetic constraints on the extent of Cenozoic rocks within the Nefza-Tabarka region, northwestern Tunisia. *J. Volcanol. Geotherm. Res.* **2003**, *122*, 51–68. [CrossRef]
9. Decrée, S.; Marignac, C.; Liégeois, J.-P.; Yans, J.; Ben Abdallah, R.; Demaiffe, D. Miocene magmatic evolution in the Nefza district (Northern Tunisia) and its relationship with the genesis of polymetallic mineralizations. *Lithos* **2014**, *192–195*, 240–258.
10. Decrée, S.; De Putter, T.; De Jong, J.; Marignac, C.; Yans, J. Iron and trace elements cycling in mineralized paleoalterites from NW Tunisia. In Proceedings of the Goldschmidt Conference 2008, Vancouver, BC, Canada, 13–18 July 2008.
11. Roman, F.; Solignac, M. Découverte d'un gisement de Mammifères pontiens à Douahria (Tunisie septentrionale). *Comptes Rendus de l'Académie des Sci.* **1934**, *199*, 1649–1659.
12. Rouvier, H.; Perthuisot, V.; Mansouri, A. Pb-Zn deposits and salt-bearing diapirs in Southern Europe and North Africa. *Econ. Geol.* **1985**, *80*, 666–687. [CrossRef]
13. Bouaziz, S.; Barrier, E.; Soussi, M.; Turki, M.M.; Zouari, H. Tectonic evolution of the northern African margin in Tunisia from paleostress data and sedimentary record. *Tectonophysics* **2002**, *357*, 227–253. [CrossRef]
14. Decrée, S.; Marignac, C.; Abidi, R.; Jemmali, N.; Deloule, E.; Souissi, F. Tectonomagmatic Context of Sedex Pb–Zn and Polymetallic Ore Deposits of the Nappe Zone Northern Tunisia, and Comparisons with MVT Deposits in the Region. In *Mineral Deposits of North Africa*; Bouabdellah, M., Slack, J.F., Eds.; Springer International Publishing: Cham, Switzerland, 2016; pp. 497–525.
15. Riahi, S.; Soussi, M.; Bou Khalfa, K.; Ben Ismail-Lattrache, K.; Stow, D.; Khomsi, S.; Bedir, M. Stratigraphy, sedimentology and structure of the Numidian flysch thrust belt in northern Tunisia. *J. Afr. Earth Sci.* **2010**, *57*, 109–126.
16. Rouvier, H. *Notice Explicative de la Carte Géologique de la Tunisie au 1:50.000 Nefza, feuille n°10 (Notice)*; Office National des Mines, Direction de la Géologie: Tunis, Tunisia, 1994.
17. Rouvier, H. Géologie de L'extrême Nord-Tunisien: Tectoniques et Paléogéographie Superposées à L'extrémité Orientale de la chaîne Nord-Maghrebine. Ph.D. Thesis, Université Pierre et Marie Curie-Paris VI, Paris, France, 1977.
18. Guérin, C. *Diceros douariensis* nov. sp., un rhinocéros du Mio-Pliocène de Tunisie du Nord. *Doc. du Lab. de Géologie de la Fac. des Sci. Lyon* **1966**, *16*, 1–50.
19. Geraads, D. Rhinocerotidae. In *Cenozoic Mammals of Africa*; Werdelin, L., Sanders, W.J., Eds.; University of California Press: Berkeley, CA, USA, 2010; pp. 669–683.
20. Harris, J.; Solounias, N.; Geraads, D. Giraffoidea. In *Cenozoic Mammals of Africa*; Werdelin, L., Sanders, W.J., Eds.; University of California Press: Berkeley, CA, USA, 2010; pp. 797–811.
21. Farley, K.A. (U–Th)/He dating: Techniques, calibrations, and applications. *Rev. Mineral. Geochem.* **2002**, *47*, 819–844. [CrossRef]
22. Allard, T.; Gautheron, C.; Bressan Riffel, S.; Balan, E.; Soares, B.F.; Pinna-Jamme, R.; Derycke, A.; Morin, G.; Bueno, G.T.; do Nascimento, N. Combined dating of goethites and kaolinites from ferruginous duricrusts. Deciphering the Late Neogene erosion history of Central Amazonia. *Chem. Geol.* **2018**, *479*, 136–150. [CrossRef]
23. Monteiro, H.; Vasconcelos, P.M.; Farley, K.A.; Spier, C.A.; Mello, C.L. (U-Th)/He geochronology of goethite and the origin and evolution of cangas. *Geochim. Cosmoch. Acta* **2014**, *131*, 267–289. [CrossRef]
24. Riffel, S.B.; Vasconcelos, P.M.; Carmo, I.O.; Farley, K.A. Goethite (U–Th)/He geochronology and precipitation mechanisms during weathering of basalts. *Chem. Geol.* **2016**, *446*, 18–32. [CrossRef]
25. Ketcham, R.A.; Gautheron, C.; Tassan-Got, L. Accounting for long alpha-particle stopping distances in (U-Th-Sm)/He geochronology: Refinement of the baseline case. *Geochim. Cosmochim. Acta* **2011**, *75*, 7779–7791. [CrossRef]
26. Ault, A.K.; Gautheron, C.; King, G.E. Innovations in (U-Th)/He, fission-track, and trapped-charge thermochronometry with applications to earthquakes, weathering, surface-mantle connections, and the growth and decay of mountains. *Tectonics* **2019**, *38*, 3705–3739. [CrossRef]
27. Shuster, D.; Vasconcelos, P.; Heim, J.; Farley, K.A. Weathering geochronology by (U-Th)/He dating of goethite. *Geochim. Cosmochim. Acta* **2005**, *69*, 659–673. [CrossRef]
28. De Putter, T.; Ruffet, G.; Yans, J.; Mees, F. The age of supergene manganese deposits in Katanga and its implications for the Neogene evolution of the African Great Lakes Region. *Ore Geol. Rev.* **2015**, *71*, 350–362. [CrossRef]
29. Verhaert, M.; Madi, A.; El Basbas, A.; El Harkaty, M.; Oummouch, A.; Oumohou, L.; Malfliet, A.; Maacha, L.; Yans, J. Genesis of an As-Pb-rich supergene mineralization: The Tazalaght and Agoujgal Cu deposits (Moroccan Anti-Atlas Copperbelt). *Econ. Geol.* **2020**, *115*, 1725–1748. [CrossRef]
30. Bellon, N. Séries Magmatiques Néogènes et Quaternaires du Pourtour de la Méditerranée Occidentale Comparées Dans Leur Cadre Géodynamique: Implications Géodynamiques. Ph.D. Thesis, Université Paris-Sud/Orsay, Orsay, France, 1976.

31. Pallary, P. Sur les mollusques fossiles terrestres, lacustres et saumâtres de l'Algérie. *Mém. Soc. Géol. France* **1901**, *22*, 1–213.
32. Bank, R.A.; Menkhorst, P.M.G. A revised bibliography of the malacological papers of Paul Pallary. *Zool. Meded.* **2009**, *Leiden 83*, 537–546.
33. Sanz-Rubio, E.; Sánchez-Moral, S.; Cañaveras, J.C.; Calvo, J.P.; Rouchy, J.M. Calcitization of Mg–Ca carbonate and Ca sulphate deposits in a continental Tertiary Basin (Calatayud Basin, NE Spain). *Sediment. Geol.* **2001**, *140*, 123–142. [CrossRef]
34. Ben Abdallah, R.; Medhioub, M.; Hatira, N.; Chaftar, H.R.; Baele, J.-M.; Yans, J.; Jamoussi, F. Hydrothermal and meteoric alteration of Triassic materials in the Oued Belif structure (Nefza, Northern Tunisia). *Eur. J. Sci. Res.* **2013**, *98*, 470–480.
35. Garnit, H.; Boni, M.; Buongiovanni, G.; Arfè, G.; Mondillo, N.; Joachimski, M.; Bouhlel, S.; Balassone, G. C-O stable isotopes geochemistry of Tunisian nonsulfide zinc deposits: A first look. *Minerals* **2018**, *8*, 13. [CrossRef]
36. Bruyère, D.; De Putter, T.; Decrée, S.; Dupuis, C.; Fuchs, Y.; Jamoussi, F.; Perruchot, A.; Arbey, F. Miocene karsts and associated Fe–Zn-rich minerals in Aïn Khamouda (Central Tunisia). *J. Afr. Earth Sci.* **2009**. [CrossRef]
37. Maher, K.; Chamberlain, C.P. Hydrologic regulation of chemical weathering and the geologic carbon cycle. *Science* **2014**, *343*, 1502–1504. [CrossRef]
38. Beauvais, A.; Chardon, D. Modes, tempo, and spatial variability of Cenozoic cratonic denudation: The West African example. *Geochem. Geophys. Geosyst.* **2013**, *14*, 1590–1608. [CrossRef]
39. Chardon, D.; Grimaud, J.L.; Rouby, D.; Beauvais, A.; Christophoul, F. Stabilization of large drainage basins over geological time scales: Cenozoic West Africa, hot spot swell growth, and the Niger River. *Geochem. Geophys. Geosyst.* **2016**, *17*, 1164–1181. [CrossRef]
40. De Menocal, P.B.; Ortiz, J.; Guilderson, T.; Adkins, J.; Sarnthein, M.; Baker, L.; Yarusinsky, M. Abrupt onset and termination of the African Humid Period: Rapid climate responses to gradual insolation forcing. *Quatern. Sci. Rev.* **2000**, *19*, 347–361. [CrossRef]
41. Gladstone, R.; Flecker, R.; Valdes, P.; Lunt, D.; Marckwick, P. The Mediterranean hydrologic budget from a Late Miocene global climate simulation. *Palaeogeogr. Palaeoclimatol. Palaeoecol.* **2007**, *251*, 254–267. [CrossRef]
42. Pound, M.J.; Haywood, A.M.; Salzmann, U.; Riding, J.B.; Lunt, D.J.; Hunter, S.J. A Tortonian (Late Miocene, 11.61–7.25Ma) global vegetation reconstruction. *Palaeogeogr. Palaeoclimatol. Palaeoecol.* **2011**, *300*, 29–45. [CrossRef]
43. Quan, C.; Liu, Y.-S.; Tang, H.; Utescher, T. Miocene shift of European atmospheric circulation from trade wind to westerlies. *Sci. Rep.* **2014**, 4. [CrossRef] [PubMed]
44. Griffin, D.L. Aridity and humidity: Two aspects of the late Miocene climate of North Africa and the Mediterranean. *Palaeogeogr. Palaeoclimatol. Palaeoecol.* **2002**, *182*, 65–91. [CrossRef]
45. Fontaine, L.; De Putter, T.; Bernard, A.; Decrée, S.; Cailteux, J.; Wouters, J.; Yans, J. Complex mineralogical-geochemical sequences in the supergene ore of the Cu-Co Luiswishi deposit (Katanga, D.R. Congo). *J. Afr. Earth Sci.* **2020**, *161*, 103674. [CrossRef]
46. De Putter, T.; Ruffet, G. Supergene manganese ore records 75 Myr-long Campanian to Pleistocene geodynamic evolution and weathering history of the Central African Great Lakes Region–Tectonics drives, climate assists. *Gondwana Res.* **2020**, *83*, 96–117. [CrossRef]
47. Dekoninck, A.; Monié, P.; Blockmans, S.; Hatert, F.; Rochez, G.; Yans, J. Genesis and $^{40}Ar/^{39}Ar$ dating of K-Mn oxides from the Stavelot Massif (Ardenne, Belgium): New insights on Oligocene to Pliocene weathering periods in Europe. *Ore Geol. Rev.* **2019**, *115*, 103191. [CrossRef]
48. Choulet, F.; Charles, N.; Barbanson, L.; Branquet, Y.; Sizaret, S.; Ennaciri, A.; Badra, L.; Chena, Y. Non-sulfide zinc deposits of theMoroccan High Atlas: Multi-scale characterization and origin. *Ore Geol. Rev.* **2014**, *56*, 115–140. [CrossRef]
49. Verhaert, M.; Bernard, A.; Dekoninck, A.; Lafforgue, L.; Saddiqi, O.; Yans, J. Mineralogical and geochemical characterization of supergene Cu-Pb-Zn-V ores in the Oriental High Atlas, Morocco. *Mineral. Depos.* **2017**, *52*, 1049–1062. [CrossRef]
50. Dekoninck, A.; Ruffet, G.; Missenard, Y.; Parizot, O.; Magoua, M.; Mouttaqi, A.; Rochez, G.; Yans, J. Multistage genesis of late Cretaceous manganese karst-hosted deposits along the High Atlas (Morocco) based on the Tasdremt case study (Souss Basin). *Miner. Depos.* **2020**. [CrossRef]
51. Velasco, F.; Herrero, J.-M.; Suárez, S.; Yusta, I.; Alvaro, A.; Tornos, F. Supergene features and evolution of gossans capping massive sulphide deposits in the Iberian Pyrite Belt. *Ore Geol. Rev.* **2013**, *53*, 181–203. [CrossRef]
52. Capella, W.; Flecker, R.; Hernández-Molina, F.J.; Simon, D.; Meijer, P.T.; Rogerson, M.; Sierro, F.J.; Krijgsman, W. Mediterranean isolation preconditioning the Earth System for late Miocene climate cooling. *Sci. Rep.* **2019**, *9*, 3795. [CrossRef] [PubMed]
53. van Hinsbergen, D.J.J.; Vissers, R.L.M.; Spakman, W. Origin and consequences of western Mediterranean subduction, rollback, and slab segmentation. *Tectonics* **2014**, *33*, 393–419. [CrossRef]
54. Osborn, H.-F. Phylogeny of the rhinoceroses of Europe. *Bull. Am. Mus. Nat. Hist.* **1900**, *13*, 229–267.
55. Antoine, P.-O.; Saraç, G. The late Miocene mammalian locality of Akkasdagi, Turkey: Rhinocerotidae. *Geodiversitas* **2005**, *27*, 601–632.
56. Gaudry, A.; Lartet, E. Sur les résultats des recherches paléontologiques entreprises dans l'Attique sous les auspices de l'Académie. *C. R. Séances Acad. Sci.* **1856**, *43*, 271–274.
57. Böhme, M.; Spassov, N.; Ebner, M.; Geraads, D.; Hristova, L.; Kirscher, U.; Kötter, S.; Linnemann, U.; Prieto, J.; Roussiakis, S.; et al. Messinian age and savannah environment of the possible hominin *Graecopithecus* from Europe. *PLoS ONE* **2017**, *12*, e0177347. [CrossRef]
58. Werdelin, L. Chronology of Neogene mammal localities. In *Cenozoic Mammals of Africa*; Werdelin, L., Ed.; University of California Press: Berkeley, CA, USA, 2010; pp. 27–43.

59. Lihoreau, F.; Barry, J.; Blondel, C.; Chaimanee, Y.; Jaeger, J.-J.; Brunet, M. Anatomical revision of the genus *Merycopotamus* (Artiodactyla; Anthracotheriidae): Its significance on late Miocene mammal dispersions in Asia. *Palaeontology* **2007**, *50*, 503–524. [CrossRef]
60. Holroyd, P.A.; Lihoreau, F.; Gunnell, G.F.; Miller, E.R.; Werdelin, L.; Sanders, W.J. Anthracotheriidae. In *Cenozoic Mammals of Africa*; Werdelin, L., Ed.; University of California Press: Berkeley, CA, USA, 2010; pp. 843–851.
61. Lihoreau, F.; Boisserie, J.-R.; Blondel, C.; Jacques, L.; Likius, A.; Mackaye, H.T.; Vignaud, P.; Brunet, M. Description and palaeobiology of a new species of *Libycosaurus* (Cetartiodactyla, Anthracotheriidae) from the Late Miocene of Toros-Menalla, northern Chad. *J. System. Palaeont.* **2014**, *12*, 761–798. [CrossRef]
62. Black, C. A new species of *Merycopotamus* (Artiodactyla: Anthracotheriidae) from the late Miocene of Tunisia. Notes du Service Géologique de Tunisie 37. *Travaux de Géologie Tunisienne* **1972**, *6*, 5–39.
63. Lihoreau, F.; (University of Montpellier, Montpellier, France). Personal communication, 2018.
64. Guérin, C. The Neogene rhinoceroses of Namibia. *Palaeontol. Afr.* **2000**, *36*, 119–138.
65. Antoine, P.-O.; Orliac, M.J.; Albayrak, E.; Ulusoy, I.; Şen, E.; Çubukçu, E.; Atıcı, G.; Aydar, E.; Sen, S. A Rhinocerotid Skull Cooked-to-Death in a 9.2 Ma-old Ignimbrite Flow of South Central Anatolia, Turkey. *PLoS ONE* **2012**. [CrossRef] [PubMed]
66. Antoine, P.-O. *Phylogénie et Évolution des Elasmotheriina (Mammalia, Rhinocerotidae)*; Mémoires du Muséum National d'Histoire Naturelle: Paris, France, 2002; Volume 188, p. 359.
67. Antoine, P.-O. Middle Miocene elasmotheriine Rhinocerotidae from China and Mongolia: Taxonomic revision and phylogenetic relationships. *Zool. Scripta* **2003**, *32*, 95–118. [CrossRef]
68. Handa, N.; Nakatsukasa, M.; Kunimatsu, Y.; Nakaya, H. A new Elasmotheriini (Perissodactyla, Rhinocerotidae) from the upper Miocene of Samburu Hills and Nakali, northern Kenya. *Geobios* **2017**, *50*, 197–209. [CrossRef]
69. Aguirre, E.; Guérin, C. Première découverte d'un Iranotheriinae (Mammalia, Perissodactyla, Rhinocerotidae) en Afrique: *Kenyatherium bishopi* nov. gen. nov. sp. de la formation vallésienne (Miocène supérieur) de Nakali (Kénya). *Estudios geologicos* **1974**, *30*, 229–233.
70. Guérin, C.; Pickford, M. *Ougandatherium napakense* nov. gen. nov. sp., le plus ancien Rhinocerotidae Iranotheriinae d'Afrique. *Ann. Paléontol.* **2003**, *89*, 1–35. [CrossRef]
71. Geraads, D.; Lehmann, T.; Peppe, D.J.; McNulty, K.P. New Rhinocerotidae from the Kisingiri localities (lower Miocene of Western Kenya). *J. Vertebr. Pal.* **2016**. [CrossRef]
72. Van Couvering, J.A.; Delson, E. African Land Mammal Ages. *J. Vert. Paleont.* **2020**, *40*, e1803340. [CrossRef]